

This is a repository copy of *Role of relativistic laser intensity on Isochoric heating of metal wire targets*.

White Rose Research Online URL for this paper:

<https://eprints.whiterose.ac.uk/id/eprint/174778/>

Version: Published Version

Article:

Martynenko, A. S., Pikuz, S. A., Antonelli, L. orcid.org/0000-0003-0694-948X et al. (13 more authors) (2021) Role of relativistic laser intensity on Isochoric heating of metal wire targets. Optics Express. pp. 12240-12251. ISSN: 1094-4087

<https://doi.org/10.1364/OE.415091>

Reuse





Other licence.

Takedown

If you consider content in White Rose Research Online to be in breach of UK law, please notify us by emailing eprints@whiterose.ac.uk including the URL of the record and the reason for the withdrawal request.



Role of relativistic laser intensity on isochoric heating of metal wire targets

A. S. MARTYENKO,^{1,11}  S. A. PIKUZ,^{1,2,12}  L. ANTONELLI,³  F. BARBATO,⁴ G. BOUTOUX,^{4,5} L. GIUFFRIDA,⁶ J. J. HONRUBIA,⁷ E. HUME,³ J. JACOBY,⁸ D. KHAGHANI,⁹  K. LANCASTER,³ P. NEUMAYER,¹⁰ O. N. ROSMEJ,¹⁰ J. J. SANTOS,⁴ O. TURIANSKA,⁴ AND D. BATANI^{2,4}

¹Joint Institute for High Temperatures of Russian Academy of Sciences, 125412 Moscow, Russia

²National Research Nuclear University MEPhI, Kashirskoe Sh. 31, 115409 Moscow, Russia

³York Plasma Institute, The University of York, Heslington, York YO10 5DQ, United Kingdom

⁴Université de Bordeaux, CNRS, CEA, CELIA, UMR 5107, F-33405, Talence, France

⁵Presently at CEA, DAM, DIF, F-91297 Arpajon Cedex, France

⁶Institute of Physics of the CAS, ELI Beamlines, Na Slovance 2, 18221 Prague, Czech Republic

⁷ETSI Aeronauticos, Universidad Politécnica de Madrid - Madrid, Spain

⁸Plasma Physics Group, Institute of Applied Physics, Goethe University, Frankfurt am Main, 60438, Germany

⁹SLAC National Accelerator Laboratory, 2575 Sand Hill Road, Menlo Park, California 94025, USA

¹⁰Plasma Physics Department, GSI Helmholtzzentrum für Schwerionenforschung, 64291 Darmstadt, Germany

¹¹artmarty@mail.ru

¹²spikuz@gmail.com

Abstract: In a recent experimental campaign, we used laser-accelerated relativistic hot electrons to ensure heating of thin titanium wire targets up to a warm dense matter (WDM) state [EPL **114**, 45002 (2016)]. The WDM temperature profiles along several hundred microns of the wire were inferred by using spatially resolved X-ray emission spectroscopy looking at the Ti K_{α} characteristic lines. A maximum temperature of ~ 30 eV was reached. Our study extends this work by discussing the influence of the laser parameters on temperature profiles and the optimisation of WDM wire-based generation. The depth of wire heating may reach several hundreds of microns and it is proven to be strictly dependent on the laser intensity. At the same time, it is quantitatively demonstrated that the maximum WDM temperature doesn't appear to be sensitive to the laser intensity and mainly depends on the deposited laser energy considering ranges of 6×10^{18} – 6×10^{20} W/cm² and 50–200 J.

© 2021 Optical Society of America under the terms of the [OSA Open Access Publishing Agreement](#)

1. Introduction

Warm dense matter (WDM) studies [1] are currently receiving increasing attention being important for various fields of science such as astrophysics, physics of plasmas and thermonuclear fusion [2–7]. WDM is usually defined as matter with density and temperature of about 0.1–100 g/cm³ and 1–100 eV, respectively. Over-dense WDM is created in laboratories by compression and heating of matter by shock waves, as has been demonstrated in various experiments on high-power lasers [8–11] or even combined with diamond anvils [12,13]. Fast isochoric heating of solid matter may ensure obtaining a near-solid-density WDM. Such experiments can be performed with XFEL [14,15], optical lasers [16–19], accelerated particle beams [20–25] and laser wakefield [26–29]. Isochoric heating of solid-state foils by optical laser pulses is a well-established way for producing WDM [30–34], however recently alternative target types have been successfully employed as well [35–41].

In our previous work in Ref. [42], thin titanium wire targets were irradiated on their tip by a high-intensity optical laser resulting in the acceleration of electrons up to relativistic energies. These hot electrons (HE) propagate along 100s μm of the wire causing inner-shell ionization of Ti atoms which is then followed by emission of the characteristic X-ray Ti K_{α} line. At the same time, the hot electrons moving in the wire draws a return current of relatively low-energy electrons [43]. Both currents combined may heat matter to a few 10s of eV. Most importantly, heating and ionisation processes occur on a much faster timescale (~ 1 ps) than the hydrodynamic expansion of the wire (~ 10 ps), thereby keeping the volume constant during heating [41].

In Ref. [42] we focused on a detailed analysis of a single shot mainly using a detailed and advanced simulation tools to interpret the data. Well-established X-ray spectroscopy techniques based on the analysis of Ti K_{α} profiles [30–33] were employed to determine the WDM temperature with spatial resolution along the wire. The advantage of using wire targets is that their prolate shape ensures, the effective collimation of the electron flow, thereby providing heating to larger depths. This facilitates high convenience of plasma diagnostics and a clear spatial distinction between the emission of the WDM zone from that of the hot plasma at the laser-irradiated wire tip.

In this paper we present an extended experimental study discussing the dependence of isochoric heating of metal wires on laser parameters (namely, intensity and energy), and their influence on the hot electron distribution and therefore the WDM temperature profile.

2. Experimental setup and K_{α} profile revealing process

The experiment was conducted at the PHELIX Nd:glass ($\lambda = 1064$ nm) laser facility at the GSI Helmholtz Centre for Heavy Ion Research in Germany [44,45]. The P-polarized laser pulse was incident on the target at 22.5° , delivering a maximum energy of 210 J in ~ 0.4 ps and was focused using a f/3 off-axis parabola to a minimum focal spot of ~ 7 μm in diameter. The nominal laser spot contained 40% of the laser energy corresponding to a maximum intensity of about 6×10^{20} W/cm² on target and total power of about 0.5 PW. The use of an ultrafast parametric amplifier (uOPA) before the main amplifier enabled reaching a main pulse to laser pedestal contrast exceeding 10^{10} [46–49], thus ensuring the absence of any long-scale length preplasma in front of the solid target. The experimental scheme is shown in Fig. 1. Laser energy, focal spot diameter, and pulse duration were varied in order to get a variety of shots with different parameters as summarised in Table 1.

Table 1. Laser pulse parameters for a set of shots assuming that 40% of laser energy is contained within the nominal focal spot

Shot #	Energy	Focus spot diameter	Pulse length	Intensity ($\times 0.4$)	T_{hot} (Beg's law) [50]
	J	μm	ps	W/cm ²	MeV
1	50	30	0.5	5.7×10^{18}	0.4
2	190	30	1.9	5.7×10^{18}	0.4
3	200	30	1	1.1×10^{19}	0.5
4	210	7	0.4	5.5×10^{20}	1.8

Targets were solid Ti wires of 50 μm in diameter irradiated on their tip. To record WDM emission we employed a focusing spectrometer with spatial resolution (FSSR) [51–55] equipped with spherically bent α -quartz crystal with Miller indices 211 ($2d = 3.082$ Å) with a radius of curvature $R = 150$ mm. It was designed to record X-ray emission with high spectral resolution to continuously cover a spectral range that extends from 2.45 to 2.8 Å (4.4–5.1 keV), including Ti XXII (Ti^{21+}) Ly_{α} , Ti XXI (Ti^{20+}) $\text{He}\alpha$, and Ti $K_{\alpha 1}$, $K_{\alpha 2}$ characteristic emission lines. The spectrometer had a spatial resolution along the Z axis of the wire and a field of view of a few mm with a magnification factor of 0.3. X-ray films were used as detectors since they provide

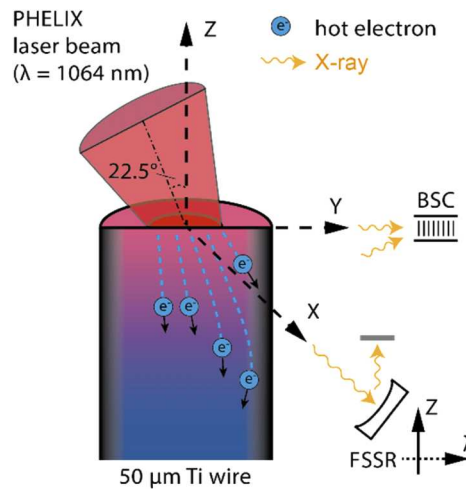


Fig. 1. Experimental scheme showing relativistic ps laser beam interaction with a $50 \mu\text{m}$ Ti wire tip and consequent isochoric matter heating by the laser-accelerated hot electron flow, resistive heating by return currents, and related processes. Laser plane of incidence (P-polarisation one) coincides with YOZ plane. BSC and FSSR were placed in XOY plane as shown.

high spatial ($\sim 20 \mu\text{m}$) and high spectral resolution ($\lambda/\delta\lambda \sim 3000$). The emission from the hot plasma corona and from the WDM region were spatially and spectrally distinguished from each other due to the significant temperature difference and to the target geometry (see Ref. [42]). Spectra showed that, in the spectral region of interest, there was no significant contribution from bremsstrahlung radiation in comparison to the characteristic emission. All spectral measurements were made in time-integrated mode. The WDM temperature profiles were retrieved based on analysis of Ti K_α X-ray emission spectra recorded with FSSR. A “bremsstrahlung cannon” hard X-ray spectrometer (BSC) was used to estimate the HE energy distribution with Monte-Carlo simulations used to back-calculate the incident bremsstrahlung radiation produced by hot electrons as described in Ref. [56–59]. In our case, the BSC was able to effectively reveal the presence of hot electrons of about 0.1–5 MeV.

HEs are laser-accelerated in the area close to the target surface, i.e. in the hot plasma volume where laser-matter interaction takes place. Consecutive HE current is complex and there are components which propagate normally to the target surface while a great fraction of HE is accelerated towards the laser direction [60–62]. Electric potential induced on the target surface prevents most of the HE from escaping, as it shown in Fig. 1 and discussed in [42]. It is assumed, that heating of deeper-lying areas of the wire are caused by HE, return currents, and other processes whereas ionisation is mainly caused by HE. However, first few 10s of microns of the wire were heated due to a bulk conductivity process. Therefore, plasma in this region is deeply ionized and its temperature is rather high reaching several hundred eVs. Though such temperature is too high for the “neutral” K_α line to be emitted, the line is also observed there in the temporally integrated spectra. In this case, the neutral K_α line is likely generated at the very early stages and comes from the rather cold regions surrounding the hot focal spot. It also should be noted that here we do not consider the initial stage of electron propagation in the target, i.e. from the laser focal spot along the laser beam axis, to the edge of the wire. This process occurs on the scale of wire diameter ($\sim 50 \mu\text{m}$), so cannot be distinguished experimentally from the hot plasma zone. We consider and discuss only heating deeper than $\sim 60 \mu\text{m}$ where the electrons are expected to move along the wire.

Experimental data processing was performed in a similar way to what described in details in Ref. [30]. Ti K_{α} profiles were spatially resolved along the wire and, they were initially compared with modelling spectra calculated with the atomic-kinetic code PrismSPECT [63,64]. However, it appeared that SCFLY [65] is more accurate in the atomic-kinetic modelling of X-ray spectra since it includes more atomic levels and configuration for low-charged ions with multiple bound electrons (see Ref. [30]); as such only the results of experimental data processing with SCFLY are shown below. Spectra were calculated assuming a 1% 0.5 MeV HE fraction. Spectral line profiles did not show any significant dependence on HE energy in a range of 0.5–2.5 MeV (which correspond to the range of hot electron energies in the performed experiment). Therefore, the same set of curves can be used to analyse our experimental data from shots with different laser intensities (i.e. regardless of the expected HE energy). All experimental spectra were time-integrated having a contribution from different stages of plasma expansion. Therefore, a two-temperature approach appeared to provide a reasonable description of experimental data [30,66]. WDM temperature was estimated as a sum of relatively low T_{bulk}^{low} and high T_{bulk}^{high} temperatures (with a fraction $a = 0..1$): $T_{bulk}^{avg} = aT_{bulk}^{low} + (1 - a)T_{bulk}^{high}$. Typically, a was in a range of 0.4–0.6 and $T_{bulk}^{low}/T_{bulk}^{high}$ was about 1.5–2. For example, $a = 0.6$, $T_{bulk}^{low} = 20$ eV, $T_{bulk}^{high} = 30$ eV for shot #3 at 100 μm position, see Fig. 2. The position in space where Ti K_{α} total emission reaches its maximum was considered as the laser-target interaction point and was set to be a “0 μm ” position on Z axis. A similar yet simplified method was previously used for revelling temperature profiles shown in Ref. [42]. The found temperature profiles are displayed in Fig. 2 and discussed in detail in the next section.

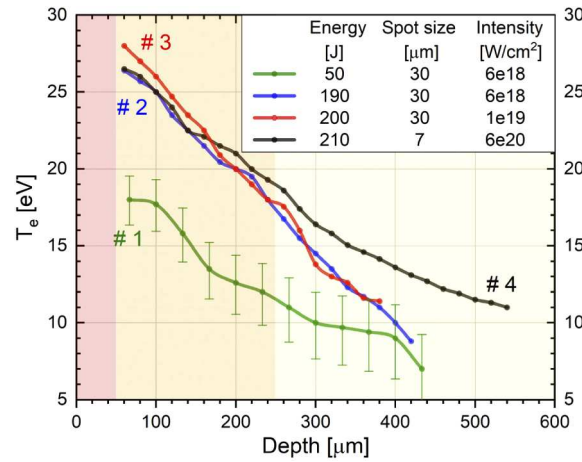


Fig. 2. Experimental temperature profiles of WDM generated inside the titanium retrieved from analysis of its K_{α} emission for the shots listed in Table 1. For ease of comparison error bars are indicated for shot #1 only. Profiles were retrieved along the axes OZ in Fig. 1; “0 μm ” corresponds to the laser-target interaction point, though the direction is opposed.

3. Results and discussion

Let us discuss the influence of laser energy and intensity on laser-accelerated HE energy distribution. In general, HE energy spectrum can be roughly described by a Maxwellian distribution with a characteristic temperature T_{hot} [67], which may be estimated according to the laser intensity value using a semi-empirical scaling law. Here we used a modified Beg’s law for high intensity range according to Ref. [50], $T_{hot}[\text{MeV}] = 1.01 \cdot (I\lambda^2/10^{18})^{\frac{1}{3}}$, where I [W/cm²] and λ [μm] are laser intensity and wavelength, accordingly. It is shown with a black

curve in Fig. 3(a). Following it, increasing the laser intensity while keeping the laser energy fixed leads to increasing T_{hot} and the related HE energy redistribution. In turn, increasing laser energy while keeping laser intensity fixed leads to increasing the full energy deposited to HE component while it does not significantly change T_{hot} . One should therefore expect a more effective target heating despite the same T_{hot} . In order to prove these statements let's compare two different experimental shots (#1 and #2 in Table 1) in which we varied the laser energy while keeping the laser intensity constant. Here the laser energies were different by a factor of four, the focal spot was not changed and the laser intensities were kept constant maintained fixed by varying the laser pulse duration: $E_2/E_1 \sim 4$ and $I_1 \sim I_2$, as specified in Table 1. HE temperature and full energy of HE for these shots are shown in Fig. 3(a) and (b), respectively. As expected, the low-energy shot #1 generated almost half as much HE as the high-energy shot #2, while the T_{hot} values for those shots are roughly equal within the measurement's accuracy. This has a certain influence on the temperature profile of hot matter, as shown by the green and blue curves for shots #1 and #2, respectively, in Fig. 2. The two profiles noticeably lie in different temperature regions. Maximum temperatures at 60 μm depth are about 18 and 28 (± 1.5) eV for low-energy shot #1 and for the high-energy shot #2, respectively. Both profiles reveal a linear decrease of WDM temperature up to a maximum distinguishable heating depth of about 400 μm . A similar dynamic is expected for deeper lying layers (depth > 400 μm), although it was not experimentally revealed due to the low signal-to-noise ratio in this region. The experimental results confirm our earlier statement regarding the role of laser energy on HE temperature and on their full energy.

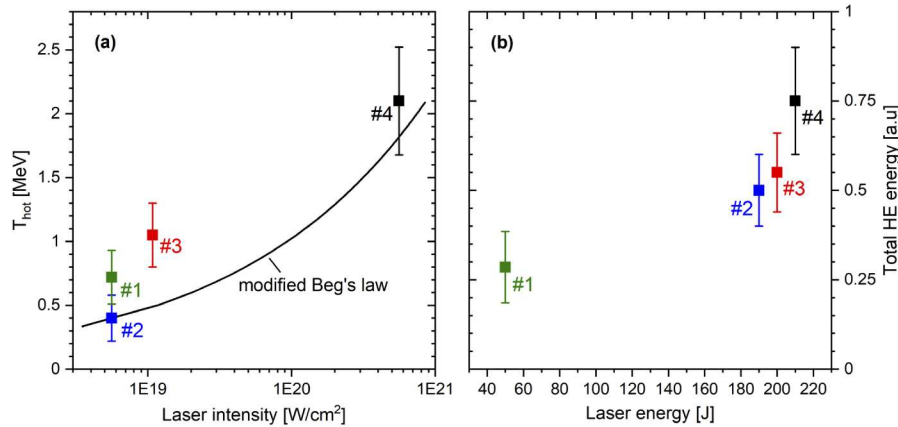


Fig. 3. (a) Hot electron temperatures and (b) total hot electron energy for the shots listed in Table 1. Experimental values were revealed based on a “bremsstrahlung cannon” hard X-ray spectrometer and are marked with black dots. The black curve corresponds to the modified semi-empirical Bag’s law (according to Ref. [50]).

The change in laser intensity is reflected differently in target heating. This can be seen by comparing the experimental results (temperature profiles) for the shots #2 and #3 shown in Fig. 2. Here the laser intensities were changed by a factor of two while laser energies remained approximately the same, $I_3/I_2 \sim 2$ and $E_3 \sim E_2$. We see that the temperature profiles are nearly coincident in the whole observed region. This is also in agreement with HE parameters revealed from BSC. HE electron temperatures and full energy are equal within the measurement error bars, as indicated in Fig. 3(a) and (b). This illustrates that the increase of laser intensity by a factor of two is not enough to produce a significant change of energy deposited by HE, i.e. to produce an increase of WDM temperature and depth of heating, at least for the considered range of intensities. To provide a basic interpretation and qualitative description of discussed experimental results we implement a simple physical approach which considers interaction of HE of different energies

with matter. We made Monte-Carlo GEANT4 [68,69] simulations consider heating of a Ti solid-state laterally infinite material block by HE of different energies injected normal to the target surface. Though, initially in experiment HE start to propagate with some angular distribution along a laser axis, electric potential induced on the target surface prevents HE from escaping and redirects them to move along the wire [70]. Therefore, considering the HE propagation and matter heating many hundreds of microns deep into the target we simulate the process by injecting HE without initial divergence. Figure 4(a) shows the energy deposited in solid Ti by Hs of different energies as a function of depth. The higher the HE energy, the lower its collisional frequency [71]. It is clearly seen that the depth corresponding to peak energy deposition increases with HE energy, while the temperature profiles become smoother. Figure 4(a) shows that HEs of energy < 1 MeV must be the main heating source of matter up to ~ 250 μm depth (orange area in Fig. 4). A deeper lying target region marked in yellow corresponds to target regions mainly heated by HEs with energies > 1 MeV. Beg's law suggests that the greater the laser intensity, the larger the T_{hot} value. Despite the fact that low energy electrons always dominate in the electron energy spectrum, the number of relatively high energy HEs increases for higher values of T_{hot} , as demonstrated in Fig. 4(b), which shows the dependence on depth of energy deposited by HE fluxes having a Maxwellian distribution for different T_{hot} (the total electron energy was set to be the same for all curves). It is clear that the temperature curves for $T_{\text{hot}} \geq 1$ MeV don't undergo dramatic changes for relatively small increase of T_{hot} (i.e. of laser intensity).

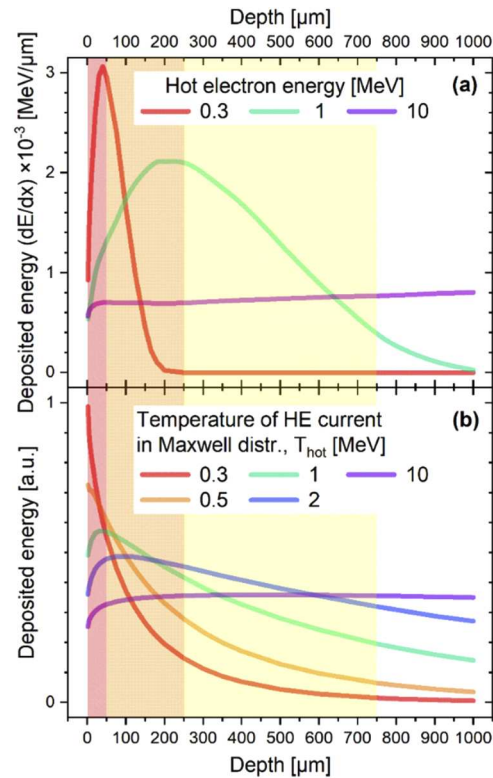


Fig. 4. (a) Dependence of energy deposited in solid-state Ti by single hot electrons on the layer depth calculated in GEANT4 toolkit for various hot electron energies. (b) Calculated total deposited energy in solid-state Ti by a hot electron current having a single-temperature Maxwell distribution energy spectrum. Total electron energies were set to be the same for all cases. The target was considered as a solid-state, laterally infinite material block. The effect of the confinement of hot electron flow due to the wire geometry was not considered.

When increasing the laser intensity even further (whilst keeping the laser energy on target constant), one can expect changes in the WDM temperature profile and an effective heating of the target to deeper lying layers. This is demonstrated by comparing the green and blue curves for $T_{hot} = 1$ and 2 MeV in Fig. 4(b). The energy deposition in the region 0–300 μm is roughly the same, while the difference is more pronounced in the region 300–1000 μm . The experimental temperature profiles for shots #2 and #4 confirm these expectations. The laser intensity here was increased by a factor of 100 while the energy was constant, $I_4/I_2 \sim 100$ and $E_4 \sim E_2$. The T_{hot} values for shots #4 and #2 were measured to be 2.1 (± 0.4) and 0.4 (± 0.2) MeV, respectively, see Fig. 3(a), which is in general agreement with Beg's law (while the estimated HE full energy changes by a factor of 1.5), see Fig. 3(b). The WDM temperature profiles for these shots are equal within the measurement's accuracy up to depths of ~ 300 μm along the wire, see Fig. 2. This illustrates that laser pulse intensity does not significantly affect the WDM temperature profile on this spatial range. At the same time, the heating depth for high intensity shot #4 is significantly higher than that of shot #2 (see the range of ~ 300 –550 μm in Fig. 2) and in particular the WDM temperatures noticeably differ at 400 μm depth, 14 and 10 eV for shot #4 and #2, respectively. This confirms that the bigger the laser intensity, the higher the heating depth and the smoother the profile in general.

The approach we have used to explain the temperature profiles dependence on laser intensity and energy considerably simplifies the design of future experiments. It provides a good qualitative description of dynamics and of the observed dependence of WDM temperature profiles on laser parameters. However, it does not include the description of target edges and of associated effects such as the presence of induced surface currents and self-generated electromagnetic fields, influence on electron current, time evolution of these processes etc. In particular, we neglect the collimating effect due to the finite geometry of the wire. Such collective effects would change the penetration of HE in matter, their stopping ranges, and ultimately their energy deposition. However, we believe that the observations we made in our paper concerning the relative changes as a function of laser energy and intensity will remain valid. In any case, developing complete numerical models describing HE generation, penetration, and heating of matter is of great interest and the experimental results presented in our work may be used to benchmark such models. These effects were indeed taken into account at least partially in Ref. [42].

It is worth mentioning that following the discussed experimental data and simplified physical approach, it may be expected that a further increase of the laser intensity at a constant energy would lead to a significant increase of the heating depth, while the maximum WDM temperature would change slightly. Our observations also suggest that it can be possible to tune the laser pulse parameters in order to obtain a specific "desired" WDM temperature profile. Coating the wire tip with high-Z material may lead to the simultaneous decrease of T_{hot} and increase of HE number, which may increase the WDM temperature in the first few hundreds μm of the target. However, despite being in practice a very cost-intensive option, the most reliable way of increasing the wire WDM temperature is by enhancing the deposited laser energy.

The discrepancy between the maximum temperature measured in present and previous work (see Ref. [42]) should also be mentioned. This is due to the fact that we used different spectroscopic codes for analysing spectra which provided more accurate description of experimental data. Most likely, the previous temperature values from [42] were overestimated by a factor ~ 2 . However, although quantitatively important, the presented data show the same qualitative trends and therefore this does not affect the conclusion of our paper.

4. Conclusions

In this article, we experimentally studied the influence of laser pulse parameters on temperature profiles of WDM generated in a titanium wire heated by a laser-accelerated hot-electron current. Laser intensity and energy were varied in ranges of 6×10^{18} – 6×10^{20} W/cm² and 50–200 J,

respectively. The increase in laser energy (while keeping intensity constant) leads to an increase in the total HE energy and to the subsequent rise of WDM temperature in the first few hundred microns of the target. Beyond laser intensities of about 1×10^{19} W/cm² (which corresponds to ~ 1 MeV characteristic temperature of hot electron distribution), the maximum WDM temperature becomes weakly sensitive to the laser intensity and mainly depends on the deposited energy. On the other hand, an increase of laser intensity at constant laser energy leads to heating of deeper target layers. These dependencies are explained with basic physical principles and simplified numerical simulation of HE flows and WDM heating to show the influence of laser parameters on the WDM temperature profile. Our experimental data may also be used to construct and verify more complex models of WDM heating by laser-accelerated HEs in further studies.

Funding. Ministry of Science and Higher Education of the Russian Federation (075 15 2020 785); H2020 Euratom (633053, ENR-IFE19.CEA-01).

Acknowledgments. We would like to acknowledge the support from the PHELIX laser team. The work of JIHT RAS team was supported by The Ministry of Science and Higher Education of the Russian Federation (Agreement with Joint Institute for High Temperatures RAS No 075 15 2020 785). This work has been carried out within the framework of the EUROfusion Consortium and has received funding from the Euratom research and training programme 2014-2018 and 2019-2020 under grant agreement No 633053. The views and opinions expressed herein do not necessarily reflect those of the European Commission. The involved teams have operated within the framework of the Enabling Research Project: ENR-IFE19.CEA-01 «Study of Direct Drive and Shock Ignition for IFE: Theory, Simulations, Experiments, Diagnostics development».

Disclosures. The authors declare no conflicts of interest.

References

1. D. Batani, "Matter in extreme conditions produced by lasers," *EPL* **114**(6), 65001 (2016).
2. R. Betti and O. A. Hurricane, "Inertial-confinement fusion with lasers," *Nat. Phys.* **12**(5), 435–448 (2016).
3. D. Batani, S. Baton, A. Casner, S. Depierreux, M. Hohenberger, O. Klimo, M. Koenig, C. Labaune, X. Ribeyre, C. Rousseaux, G. Schurtz, W. Theobald, and V. T. Tikhonchuk, "Physics issues for shock ignition," *Nucl. Fusion* **54**(5), 054009 (2014).
4. G. A. Mourou, T. Tajima, and S. V. Bulanov, "Optics in the relativistic regime," *Rev. Mod. Phys.* **78**(2), 309–371 (2006).
5. J. E. Bailey, T. Nagayama, G. P. Loisel, G. A. Rochau, C. Blancard, J. Colgan, P. Cosse, G. Faussurier, C. J. Fontes, F. Gilleron, I. Golovkin, S. B. Hansen, C. A. Iglesias, D. P. Kilcrease, J. J. MacFarlane, R. C. Mancini, S. N. Nahar, C. Orban, J.-C. Pain, A. K. Pradhan, M. Sherrill, and B. G. Wilson, "A higher-than-predicted measurement of iron opacity at solar interior temperatures," *Nature* **517**(7532), 56–59 (2015).
6. S. N. Nahar and A. K. Pradhan, "Large Enhancement in High-Energy Photoionization of Fe XVII and Missing Continuum Plasma Opacity," *Phys. Rev. Lett.* **116**(23), 235003 (2016).
7. R. P. Drake, *High-Energy-Density Physics: Fundamentals, Inertial Fusion, and Experimental Astrophysics* (2018).
8. D. J. Hoarty, P. Allan, S. F. James, C. R. D. Brown, L. M. R. Hobbs, M. P. Hill, J. W. O. Harris, J. Morton, M. G. Brookes, R. Shepherd, J. Dunn, H. Chen, E. Von Marley, P. Beiersdorfer, H. K. Chung, R. W. Lee, G. Brown, and J. Emig, "Observations of the Effect of Ionization-Potential Depression in Hot Dense Plasma," *Phys. Rev. Lett.* **110**(26), 265003 (2013).
9. L. B. Fletcher, A. L. Kritcher, A. Pak, T. Ma, T. Döppner, C. Fortmann, L. Divol, O. S. Jones, O. L. Landen, H. A. Scott, J. Vorberger, D. A. Chapman, D. O. Gericke, B. A. Mattern, G. T. Seidler, G. Gregori, R. W. Falcone, and S. H. Glenzer, "Observations of Continuum Depression in Warm Dense Matter with X-Ray Thomson Scattering," *Phys. Rev. Lett.* **112**(14), 145004 (2014).
10. H. J. Lee, P. Neumayer, J. Castor, T. Döppner, R. W. Falcone, C. Fortmann, B. A. Hammel, A. L. Kritcher, O. L. Landen, R. W. Lee, D. D. Meyerhofer, D. H. Munro, R. Redmer, S. P. Regan, S. Weber, and S. H. Glenzer, "X-Ray Thomson-Scattering Measurements of Density and Temperature in Shock-Compressed Beryllium," *Phys. Rev. Lett.* **102**(11), 115001 (2009).
11. K. Jakubowska, D. Mancelli, R. Benocci, J. Trela, I. Errea, A. S. Martynenko, P. Neumayer, O. Rosmej, B. Borm, A. Molineri, C. Verona, D. Cannatà, A. Alverdiev, H. E. Roman, and D. Batani, "Reflecting laser-driven shocks in diamond in the megabar pressure range," *High Power Laser Sci. Eng.* **9**(1), e3 (2021).
12. P. Loubeyre, P. M. Celliers, D. G. Hicks, E. Henry, A. Dewaele, J. Pasley, J. Eggert, M. Koenig, F. Occelli, K. M. Lee, R. Jeanloz, D. Neely, A. Benuzzi-Mounaix, D. Bradley, M. Bastea, S. Moon, and G. W. Collins, "Coupling static and dynamic compressions: first measurements in dense hydrogen," *High Pressure Res.* **24**(1), 25–31 (2004).
13. Z. Konôpková, R. S. McWilliams, N. Gómez-Pérez, and A. F. Goncharov, "Direct measurement of thermal conductivity in solid iron at planetary core conditions," *Nature* **534**(7605), 99–101 (2016).
14. L. B. Fletcher, H. J. Lee, T. Döppner, E. Galtier, B. Nagler, P. Heimann, C. Fortmann, S. LePape, T. Ma, M. Millot, A. Pak, D. Turnbull, D. A. Chapman, D. O. Gericke, J. Vorberger, T. White, G. Gregori, M. Wei, B. Barbrel, R. W.

- Falcone, C.-C. Kao, H. Nuhn, J. Welch, U. Zastra, P. Neumayer, J. B. Hastings, and S. H. Glenzer, "Ultrabright X-ray laser scattering for dynamic warm dense matter physics," *Nat. Photonics* **9**(4), 274–279 (2015).
15. O. Ciricosta, S. M. Vinko, B. Barbre, D. S. Rackstraw, T. R. Preston, T. Burian, J. Chalupský, B. I. Cho, H. K. Chung, G. L. Dakovski, K. Engelhorn, V. Hájková, P. Heimann, M. Holmes, L. Juha, J. Krzywinski, R. W. Lee, S. Toleikis, J. J. Turner, U. Zastra, and J. S. Wark, "Measurements of continuum lowering in solid-density plasmas created from elements and compounds," *Nat. Commun.* **7**(1), 11713 (2016).
 16. H. Nishimura, R. Mishra, S. Ohshima, H. Nakamura, M. Tanabe, T. Fujiwara, N. Yamamoto, S. Fujioka, D. Batani, M. Veltcheva, T. Desai, R. Jafer, T. Kawamura, Y. Sentoku, R. Mancini, P. Hakel, F. Koike, and K. Mima, "Energy transport and isochoric heating of a low-Z, reduced-mass target irradiated with a high intensity laser pulse," *Phys. Plasmas* **18**(2), 022702 (2011).
 17. H. Nishimura, T. Kawamura, R. Matsui, Y. Ochi, S. Okihara, S. Sakabe, F. Koike, T. Johzaki, H. Nagatomo, K. Mima, I. Uschmann, and E. Förster, "K α spectroscopy to study energy transport in ultrahigh-intensity laser produced plasmas," *J. Quant. Spectrosc. Radiat. Transfer* **81**(1-4), 327–337 (2003).
 18. E. Martinelli, M. Koenig, S. D. Baton, J. J. Santos, F. Amiranoff, D. Batani, E. Perelli-Cippo, F. Scianitti, L. Gremillet, R. Mélizzi, A. Decoster, C. Rousseaux, T. A. Hall, M. H. Key, R. Snavely, A. J. MacKinnon, R. R. Freeman, J. A. King, R. Stephens, D. Neely, and R. J. Clarke, "Fast-electron transport and heating of solid targets in high-intensity laser interactions measured by K α fluorescence," *Phys. Rev. E* **73**(4), 046402 (2006).
 19. A. S. Martynenko, S. A. Pikuz, I. Y. Skobelev, S. N. Ryazantsev, C. D. Baird, N. Booth, L. N. K. Döhl, P. Durey, A. Y. Faenov, D. Farley, R. Kodama, K. Lancaster, P. McKenna, C. D. Murphy, C. Spindloe, T. A. Pikuz, and N. Woolsey, "Optimization of a laser plasma-based x-ray source according to WDM absorption spectroscopy requirements," *Matter Radiat. Extrem.* **6**(1), 014405 (2021).
 20. J. E. Coleman, H. E. Morris, M. S. Jakulewicz, H. L. Andrews, and M. E. Briggs, "Hydrodynamic disassembly and expansion of electron-beam-heated warm dense copper," *Phys. Rev. E* **98**(4), 043201 (2018).
 21. W. Bang, B. J. Albright, P. A. Bradley, D. C. Gautier, S. Palaniyappan, E. L. Vold, M. A. S. Cordoba, C. E. Hamilton, and J. C. Fernández, "Visualization of expanding warm dense gold and diamond heated rapidly by laser-generated ion beams," *Sci. Rep.* **5**(1), 14318 (2015).
 22. P. A. Ni, M. I. Kulish, V. Mintsev, D. N. Nikolaev, V. Y. Ternovoi, D. H. H. Hoffmann, S. Udea, A. Hug, N. A. Tahir, and D. Varentsov, "Temperature measurement of warm-dense-matter generated by intense heavy-ion beams," *Laser Part. Beams* **26**(4), 583–589 (2008).
 23. W. Bang, B. J. Albright, P. A. Bradley, E. L. Vold, J. C. Boettger, and J. C. Fernández, "Uniform heating of materials into the warm dense matter regime with laser-driven quasimonoenergetic ion beams," *Phys. Rev. E* **92**(6), 063101 (2015).
 24. R. Cheng, Y. Lei, X. Zhou, Y. Wang, Y. Chen, Y. Zhao, J. Ren, L. Sheng, J. Yang, Z. Zhang, Y. Du, W. Gai, X. Ma, and G. Xiao, "Warm dense matter research at HIAF," *Matter Radiat. Extrem.* (2018).
 25. B. Y. Sharkov, D. H. H. Hoffmann, A. A. Golubev, and Y. Zhao, "High energy density physics with intense ion beams," *Matter Radiat. Extrem.* (2016).
 26. M. Šmíd, I. Gallardo González, H. Ekerfelt, J. Björklund Svensson, M. Hansson, J. C. Wood, A. Persson, S. P. D. Mangles, O. Lundh, and K. Falk, "Highly efficient angularly resolving x-ray spectrometer optimized for absorption measurements with collimated sources," *Rev. Sci. Instrum.* **88**(6), 063102 (2017).
 27. B. Mahieu, N. Jourdain, K. Ta Phuoc, F. Dorchies, J.-P. Goddet, A. Lifschitz, P. Renaudin, and L. Lecherbourg, "Probing warm dense matter using femtosecond X-ray absorption spectroscopy with a laser-produced betatron source," *Nat. Commun.* **9**(1), 3276 (2018).
 28. B. Kettle, E. Gerstmayr, M. J. V. Streeter, F. Albert, R. A. Baggott, N. Bourgeois, J. M. Cole, S. Dann, K. Falk, I. Gallardo González, A. E. Hussein, N. Lemos, N. C. Lopes, O. Lundh, Y. Ma, S. J. Rose, C. Spindloe, D. R. Symes, M. Šmíd, A. G. R. Thomas, R. Watt, and S. P. D. Mangles, "Single-Shot Multi-keV X-Ray Absorption Spectroscopy Using an Ultrashort Laser-Wakefield Accelerator Source," *Phys. Rev. Lett.* **123**(25), 254801 (2019).
 29. N. Lemos, P. King, J. L. Shaw, A. L. Milder, K. A. Marsh, A. Pak, B. B. Pollock, C. Goyon, W. Schumaker, A. M. Saunders, D. Papp, R. Polanek, J. E. Ralph, J. Park, R. Tommasini, G. J. Williams, H. Chen, F. V. Hartemann, S. Q. Wu, S. H. Glenzer, B. M. Hegelich, J. Moody, P. Michel, C. Joshi, and F. Albert, "X-ray sources using a picosecond laser driven plasma accelerator," *Phys. Plasmas* **26**(8), 083110 (2019).
 30. L. J. Bae, U. Zastra, H.-K. Chung, A. C. Bernstein, M. S. Cho, G. M. Dyer, E. Galtier, Z.-H. He, P. A. Heimann, G. B. Kang, M. Kim, Y. H. Kim, H. J. Lee, J. W. Lee, B. Nagler, A. G. R. Thomas, and B. I. Cho, "Diagnosis of warm dense conditions in foil targets heated by intense femtosecond laser pulses using K α imaging spectroscopy," *Opt. Express* **26**(5), 6294 (2018).
 31. U. Zastra, A. Sengebusch, P. Audebert, E. Brambrink, R. R. Fäustlin, T. Kämpfer, E. Kroupp, R. Loetzsch, Y. Maron, H. Reinholz, G. Röpke, E. Stambulchik, I. Uschmann, and E. Förster, "High-resolution radial K α spectra obtained from a multi-keV electron distribution in solid-density titanium foils generated by relativistic laser-matter interaction," *High Energy Density Phys.* **7**(2), 47–53 (2011).
 32. M. Šmíd, O. Renner, A. Colaitis, V. T. Tikhonchuk, T. Schlegel, and F. B. Rosmej, "Characterization of suprathermal electrons inside a laser accelerated plasma via highly-resolved K α -emission," *Nat. Commun.* **10**(1), 4212 (2019).
 33. A. Y. Faenov, J. Colgan, S. B. Hansen, A. Zhidkov, T. A. Pikuz, M. Nishiuchi, S. A. Pikuz, I. Y. Skobelev, J. Abdallah, H. Sakaki, A. Sagisaka, A. S. Pirozhkov, K. Ogura, Y. Fukuda, M. Kanasaki, N. Hasegawa, M. Nishikino, M. Kando,

- Y. Watanabe, T. Kawachi, S. Masuda, T. Hosokai, R. Kodama, and K. Kondo, "Nonlinear increase of X-ray intensities from thin foils irradiated with a 200 TW femtosecond laser," *Sci. Rep.* **5**(1), 13436 (2015).
34. A. S. Martynenko, S. A. Pikuz, I. Y. Skobelev, S. N. Ryazantsev, C. Baird, N. Booth, L. Doehl, P. Durey, A. Y. Faenov, D. Farley, R. Kodama, K. Lancaster, P. McKenna, C. D. Murphy, C. Spindloe, T. A. Pikuz, and N. Woolsey, "Effect of plastic coating on the density of plasma formed in Si foil targets irradiated by ultra-high-contrast relativistic laser pulses," *Phys. Rev. E* **101**(4), 043208 (2020).
 35. M. V. Sedov, A. Y. Faenov, A. A. Andreev, I. Y. Skobelev, S. N. Ryazantsev, T. A. Pikuz, P. Durey, L. Doehl, D. Farley, C. D. Baird, K. L. Lancaster, C. D. Murphy, N. Booth, C. Spindloe, K. Y. Platonov, P. McKenna, R. Kodama, N. Woolsey, and S. A. Pikuz, "Features of the generation of fast particles from microstructured targets irradiated by high intensity, picosecond laser pulses," *Laser Part. Beams* **37**(2), 176–183 (2019).
 36. T. Ebert, N. W. Neumann, L. N. K. Döhl, J. Jarrett, C. Baird, R. Heathcote, M. Hesse, A. Hughes, P. McKenna, D. Neely, D. Rusby, G. Schaumann, C. Spindloe, A. Tebartz, N. Woolsey, and M. Roth, "Enhanced brightness of a laser-driven x-ray and particle source by microstructured surfaces of silicon targets," *Phys. Plasmas* **27**(4), 043106 (2020).
 37. P. Wachulak, T. Fok, A. Bartnik, K. A. Janulewicz, and H. Fiedorowicz, "EXAFS of titanium LIII edge using a compact laboratory system based on a laser-plasma soft X-ray source," *Appl. Phys. B* **126**(1), 11 (2020).
 38. A. Krygier, F. Coppari, G. E. Kemp, D. B. Thorn, R. S. Craxton, J. H. Eggert, E. M. Garcia, J. M. McNaney, H.-S. Park, Y. Ping, B. A. Remington, and M. B. Schneider, "Developing a high-flux, high-energy continuum backlighter for extended x-ray absorption fine structure measurements at the National Ignition Facility," *Rev. Sci. Instrum.* **89**(10), 10F114 (2018).
 39. Y. Hu, S. Jiang, J. Zhang, Q. Xue, Z. Wang, and Q. Ye, "X-ray source improvements for EXAFS measurement on SGIII prototype facility," *AIP Adv.* **10**(5), 055313 (2020).
 40. B. Yaakobi, F. J. Marshall, T. R. Boehly, R. P. J. Town, and D. D. Meyerhofer, "Extended x-ray absorption fine-structure experiments with a laser-imploded target as a radiation source," *J. Opt. Soc. Am. B* **20**(1), 238 (2003).
 41. D. C. Hochhaus, B. Aurand, M. Basko, B. Ecker, T. Kühl, T. Ma, F. Rosmej, B. Zielbauer, and P. Neumayer, "X-ray radiographic expansion measurements of isochorically heated thin wire targets," *Phys. Plasmas* **20**(6), 062703 (2013).
 42. A. Schönlein, G. Boutoux, S. Pikuz, L. Antonelli, D. Batani, A. Debayle, A. Franz, L. Giuffrida, J. J. Honrubia, J. Jacoby, D. Khaghani, P. Neumayer, O. N. Rosmej, T. Sakaki, J. J. Santos, and A. Sauteray, "Generation and characterization of warm dense matter isochorically heated by laser-induced relativistic electrons in a wire target," *EPL* **114**(4), 45002 (2016).
 43. V. T. Tikhonchuk, "Interaction of a beam of fast electrons with solids," *Phys. Plasmas* **9**(4), 1416–1421 (2002).
 44. P. Neumayer, R. Bock, S. Borneis, E. Brambrink, H. Brand, J. Caird, E. M. Campbell, E. Gaul, S. Goette, C. Haefner, T. Hahn, H. M. Heuck, D. H. H. Hoffmann, D. Javorkova, H.-J. Kluge, T. Kuehl, S. Kunzer, T. Merz, E. Onkels, M. D. Perry, D. Reemts, M. Roth, S. Samek, G. Schaumann, F. Schrader, W. Seelig, A. Tauschwitz, R. Thiel, D. Ursescu, P. Wiewior, U. Wittrock, and B. Zielbauer, "Status of PHELIX laser and first experiments," *Laser Part. Beams* **23**(03), 385–389 (2005).
 45. V. Bagnoud, B. Aurand, A. Blazevic, S. Borneis, C. Bruske, B. Ecker, U. Eisenbarth, J. Fils, A. Frank, E. Gaul, S. Goette, C. Haefner, T. Hahn, K. Harres, H.-M. Heuck, D. Hochhaus, D. H. H. Hoffmann, D. Javorková, H.-J. Kluge, T. Kuehl, S. Kunzer, M. Kreutz, T. Merz-Mantwill, P. Neumayer, E. Onkels, D. Reemts, O. Rosmej, M. Roth, T. Stoehlker, A. Tauschwitz, B. Zielbauer, D. Zimmer, and K. Witte, "Commissioning and early experiments of the PHELIX facility," *Appl. Phys. B* **100**(1), 137–150 (2010).
 46. X. Vaisseau, A. Debayle, J. J. Honrubia, S. Hulin, A. Morace, P. Nicolaï, H. Sawada, B. Vauzour, D. Batani, F. N. Beg, J. R. Davies, R. Fedosejevs, R. J. Gray, G. E. Kemp, S. Kerr, K. Li, A. Link, P. McKenna, H. S. McLean, M. Mo, P. K. Patel, J. Park, J. Peebles, Y. J. Rhee, A. Sorokovikova, V. T. Tikhonchuk, L. Volpe, M. Wei, and J. J. Santos, "Enhanced Relativistic-Electron-Beam Energy Loss in Warm Dense Aluminum," *Phys. Rev. Lett.* **114**(9), 095004 (2015).
 47. F. Wagner, C. P. João, J. Fils, T. Gottschall, J. Hein, J. Körner, J. Limpert, M. Roth, T. Stöhlker, and V. Bagnoud, "Temporal contrast control at the PHELIX petawatt laser facility by means of tunable sub-picosecond optical parametric amplification," *Appl. Phys. B* **116**(2), 429–435 (2014).
 48. A. S. Martynenko, I. Y. Skobelev, S. A. Pikuz, S. N. Ryazantsev, C. Baird, N. Booth, L. Doehl, P. Durey, D. Farley, R. Kodama, K. Lancaster, P. McKenna, C. Murphy, C. Spindloe, T. A. Pikuz, and N. Woolsey, "Determining the short laser pulse contrast based on X-Ray emission spectroscopy," *High Energy Density Phys.* **38**, 100924 (2021).
 49. S. N. Ryazantsev, I. Y. Skobelev, A. S. Martynenko, M. A. Alkhimova, M. D. Mishchenko, M. V. Sedov, T. A. Pikuz, Y. Fukuda, H. Kiriyama, A. S. Pirozhkov, and S. A. Pikuz, "Analysis of Ly α Dielectronic Satellites to Characterize Temporal Profile of Intense Femtosecond Laser Pulses," *Crystals* **11**(2), 130 (2021).
 50. Y.-Q. Cui, W.-M. Wang, Z.-M. Sheng, Y.-T. Li, and J. Zhang, "Laser absorption and hot electron temperature scalings in laser-plasma interactions," *Plasma Phys. Control. Fusion* **55**(8), 085008 (2013).
 51. A. Y. Faenov, S. A. Pikuz, A. I. Erko, B. A. Bryunetkin, V. M. Dyakin, G. V. Ivanenkov, A. R. Mingaleev, T. A. Pikuz, V. M. Romanova, and T. A. Shelkovenko, "High-performance x-ray spectroscopic devices for plasma microsources investigations," *Phys. Scr.* **50**(4), 333–338 (1994).
 52. M. A. Alkhimova, I. Y. Skobelev, A. Y. Faenov, D. A. Arich, T. A. Pikuz, and S. A. Pikuz, "Accounting for the instrument function of crystal spectrometers operating in many reflection orders in the diagnostics of laser plasma from its continuum spectrum," *Quantum Electron.* **48**(8), 749–754 (2018).

53. E. D. Filippov, I. Y. Skobelev, G. Revet, S. N. Chen, B. Khair, A. Ciardi, D. Khaghani, D. P. Higginson, S. A. Pikuz, and J. Fuchs, "X-ray spectroscopy evidence for plasma shell formation in experiments modeling accretion columns in young stars," *Matter Radiat. Extrem.* **4**(6), 064402 (2019).
54. O. Renner and F. B. Rosmej, "Challenges of x-ray spectroscopy in investigations of matter under extreme conditions," *Matter Radiat. Extrem.* **4**(2), 024201 (2019).
55. S. N. Ryazantsev, I. Y. Skobelev, E. D. Filippov, A. S. Martynenko, M. D. Mishchenko, M. Krüs, O. Renner, and S. A. Pikuz, "Precise wavelength measurements of potassium He- and Li-like satellites emitted from the laser plasma of a mineral target," *Matter Radiat. Extrem.* **6**(1), 014402 (2021).
56. R. Nolte, R. Behrens, M. Schnurer, A. Rousse, and P. Ambrosi, "A TLD-based few-channel spectrometer for mixed photon, electron, and ion fields with high fluence rates," *Radiation Protection Dosimetry* **101**(1), 73–76 (2002).
57. Y. J. Rhee, S. M. Nam, J. Peebles, H. Sawada, M. Wei, X. Vaisseau, T. Sasaki, L. Giuffrida, S. Hulin, B. Vauzour, J. J. Santos, D. Batani, H. S. McLean, P. K. Patel, Y. T. Li, D. W. Yuan, K. Zhang, J. Y. Zhong, C. B. Fu, N. Hua, K. Li, Y. Zhang, J. Q. Zhu, I. J. Kim, J. H. Jeon, T. M. Jeong, I. W. Choi, H. W. Lee, J. H. Sung, S. K. Lee, and C. H. Nam, "Spectral tomographic analysis of Bremsstrahlung X-rays generated in a laser-produced plasma," *Laser Part. Beams* **34**(4), 645–654 (2016).
58. C. D. Chen, J. A. King, M. H. Key, K. U. Akli, F. N. Beg, H. Chen, R. R. Freeman, A. Link, A. J. Mackinnon, A. G. MacPhee, P. K. Patel, M. Porkolab, R. B. Stephens, and L. D. Van Woerkom, "A Bremsstrahlung spectrometer using k-edge and differential filters with image plate dosimeters," *Rev. Sci. Instrum.* **79**(10), 10E305 (2008).
59. B. Westover, C. D. Chen, P. K. Patel, M. H. Key, H. McLean, R. Stephens, and F. N. Beg, "Fast electron temperature and conversion efficiency measurements in laser-irradiated foil targets using a bremsstrahlung x-ray detector," *Phys. Plasmas* **18**(6), 063101 (2011).
60. Y. T. Li, J. Zhang, Z. M. Sheng, J. Zheng, Z. L. Chen, R. Kodama, T. Matsuoka, M. Tampo, K. A. Tanaka, T. Tsutsumi, and T. Yabuuchi, "High-energy electrons produced in subpicosecond laser-plasma interactions from subrelativistic laser intensities to relativistic intensities," *Phys. Rev. E* **69**(3), 036405 (2004).
61. F. Lindau, O. Lundh, A. Persson, P. McKenna, K. Osvay, D. Batani, and C.-G. Wahlström, "Laser-Accelerated Protons with Energy-Dependent Beam Direction," *Phys. Rev. Lett.* **95**(17), 175002 (2005).
62. P. Norreys, D. Batani, S. Baton, F. N. Beg, R. Kodama, P. M. Nilson, P. Patel, F. Pérez, J. J. Santos, R. H. H. Scott, V. Tikhonchuk, M. Wei, and J. Zhang, "Fast electron energy transport in solid density and compressed plasma," *Nucl. Fusion* **54**(5), 054004 (2014).
63. J. J. MacFarlane, I. E. Golovkin, P. R. Woodruff, D. R. Welch, B. V. Oliver, T. A. Mehlhorn, and R. B. Campbell, "Simulation of the ionization dynamics of aluminum irradiated by intense short-pulse lasers," in *Proceedings of Third Inertial Conference on Inertial Fusion and Science Applications 2003* (American Nuclear Society, 2004), p. 457.
64. J. J. MacFarlane, I. E. Golovkin, P. Wang, P. R. Woodruff, and N. A. Pereyra, "SPECT3D - A multi-dimensional collisional-radiative code for generating diagnostic signatures based on hydrodynamics and PIC simulation output," *High Energy Density Phys.* **3**(1-2), 181–190 (2007).
65. H.-K. Chung, M. H. Chen, and R. W. Lee, "Extension of atomic configuration sets of the Non-LTE model in the application to the K α diagnostics of hot dense matter," *High Energy Density Phys.* **3**(1-2), 57–64 (2007).
66. E. Stambulchik, V. Bernshtam, L. Weingarten, E. Kroupp, D. Fisher, Y. Maron, U. Zastra, I. Uschmann, F. Zamponi, E. Förster, A. Sengebusch, H. Reinholz, G. Röppe, and Y. Ralchenko, "Progress in line-shape modeling of K-shell transitions in warm dense titanium plasmas," in *Journal of Physics A: Mathematical and Theoretical* (2009), 42(21), p. 214056.
67. I. H. Hutchinson, *Principles of Plasma Diagnostics* (Cambridge University Press, 2002).
68. S. Agostinelli, J. Allison, K. Amako, J. Apostolakis, H. Araujo, P. Arce, M. Asai, D. Axen, S. Banerjee, G. Barrand, F. Behner, L. Bellagamba, J. Boudreau, L. Broglia, A. Brunengo, H. Burkhardt, S. Chauvie, J. Chuma, R. Chytráček, G. Cooperman, G. Cosmo, P. Degtyarenko, A. Dell'Acqua, G. Depaola, D. Dietrich, R. Enami, A. Feliciello, C. Ferguson, H. Fesefeldt, G. Folger, F. Foppiano, A. Forti, S. Garelli, S. Giani, R. Giannitrapani, D. Gibin, J. J. Gomez Cadenas, I. Gonzalez, G. Gracia Abril, G. Greeniaus, W. Greiner, V. Grichine, A. Grossheim, S. Guatelli, P. Gumplinger, R. Hamatsu, K. Hashimoto, H. Hasui, A. Heikkinen, A. Howard, V. Ivanchenko, A. Johnson, F. W. Jones, J. Kallenbach, N. Kanaya, M. Kawabata, Y. Kawabata, M. Kawaguti, S. Kelner, P. Kent, A. Kimura, T. Kodama, R. Kokoulin, M. Kossov, H. Kurashige, E. Lamanna, T. Lampen, V. Lara, V. Lefebvre, F. Lei, M. Liendl, W. Lockman, F. Longo, S. Magni, M. Maire, E. Medernach, K. Minamimoto, P. Mora de Freitas, Y. Morita, K. Murakami, M. Nagamatsu, R. Nartallo, P. Nieminen, T. Nishimura, K. Ohtsubo, M. Okamura, S. O'Neale, Y. Oohata, K. Paech, J. Perl, A. Pfeiffer, M. G. Pia, F. Ranjard, A. Rybin, S. Sadilov, E. di Salvo, G. Santin, T. Sasaki, N. Savvas, Y. Sawada, S. Scherer, S. Sei, V. Sirotenko, D. Smith, N. Starkov, H. Stoecker, J. Sulkimo, M. Takahata, S. Tanaka, E. Tcherniaev, E. Safai Tehrani, M. Tropeano, P. Truscott, H. Uno, L. Urban, P. Urban, M. Verderi, A. Walkden, W. Wander, H. Weber, J. P. Wellisch, T. Wenaus, D. C. Williams, D. Wright, T. Yamada, H. Yoshida, and D. Zschesche, "GEANT4 - A simulation toolkit," *Nucl. Instruments Methods Phys. Res. Sect. A Accel. Spectrometers, Detect. Assoc. Equip.* **506**, 250–303 (2003).
69. M. Batic, G. Hoff, M. G. Pia, P. Saracco, and G. Weidenspointner, "Validation of Geant4 Simulation of Electron Energy Deposition," *IEEE Trans. Nucl. Sci.* **60**(4), 2934–2957 (2013).
70. R. Pompili, M. P. Anania, F. Bisesto, M. Botton, M. Castellano, E. Chiadroni, A. Cianchi, A. Curcio, M. Ferrario, M. Galletti, Z. Henis, M. Petrarca, E. Schleifer, and A. Zigler, "Femtosecond dynamics of energetic electrons in high intensity laser-matter interactions," *Sci. Rep.* **6**(1), 35000 (2016).

71. J. D. Jackson and R. F. Fox, "Classical Electrodynamics," 3rd ed Am. J. Phys. **67**(9), 841–842 (1999).